Measurement and Modeling of the Phase Behavior of the (Carbon Dioxide + Water) Mixture at Temperatures From 298.15 K to 448.15 K

Shu-Xin Hou, Geoffrey C. Maitland, and J. P. Martin Trusler[*],

Qatar Carbonates and Carbon Storage Research Centre
Department of Chemical Engineering
Imperial College London, South Kensington Campus, London SW7 2AZ. U.K.

Abstract

An analytical apparatus has been designed to study the phase behavior of fluid mixtures of relevance to CO_2-enhanced oil recovery and carbon dioxide storage in deep aquifers or depleted oil fields. The fluid phases are circulated by means of a dual-channel magnetically-coupled pump and aliquots may be withdrawn from the re-circulation loops, by means of high-pressure sampling valves, for analysis by gas chromatography. The high-pressure cell is fitted with a special probe that may be rotated in order to draw liquid into the re-circulation loop from different heights within the cell, thereby permitting the study of three-phase vapor-liquid-liquid equilibria. The working temperature range of the apparatus is from (298 to 448) K and the maximum working pressure is 50 MPa.

In this work, measurements have been made on the binary system (CO_2 + H_2O) at temperatures from (298.15 K to 448.15 K) and pressure from (1.5 to 18.0 MPa), and the results are compared with the available literature data. Vapor-liquid-liquid and liquid-liquid equilibrium points were also measured at T = 298.15 K. Standard uncertainties were 0.04 K for temperature, 0.04 % of reading for pressure, and typically 3×10^{-4} and 8×10^{-4} for the mole fractions in liquid and vapor phases respectively. The results have been correlated by means of an asymmetric approach based on the Peng-Robinson equation of state, for the vapor phase, and an extended form of Henry's law incorporating the NRTL solution model, for the aqueous liquid-phase. The ability of the Krichevsky-Kasarnovsky (KK) approach to correlate the data has also been evaluated.

Keywords: Phase behavior; vapor-liquid equilibrium (VLE); vapor-liquid-liquid equilibrium (VLLE); CO_2; H_2O; Equation of state; Krichevsky-Kasarnovsky approach.

[*] To whom correspondence should be addressed. Tel: +44 (0)20 7594 5592, E-mail: m.trusler@imperial.ac.uk

1. Introduction

Phase behavior is of fundamental importance in the oil industry. For CO_2-EOR and carbon storage, the systems of interest are (CO_2 + hydrocarbons + brines) and a gap analysis indicates that the available experimental data are quite limited, especially for multi-component systems and mixtures containing brines [1]. Moreover, many experimental data are for pressures below 10 MPa and/or lack a full compositional analysis. The (CO_2 + water/brine) systems are also of great interest in geological research [2].

To understand fully the phase behavior for (CO_2 + brine) systems, knowledge of (CO_2 + H_2O) is required as a baseline. Owing to its scientific significance and industrial importance, there have been many experimental studies of this system, the earliest dating back to the 19th century, and there are also a number of literature reviews. However, significant uncertainty remains, especially at elevated temperatures and pressures, owing to quite large discrepancies between literature sources.

The (CO_2 + H_2O) system exhibits type III phase behavior in the classification of Scott and van Konynenburg [3, 4] with a discontinuous vapor-liquid critical curve, a wide region of liquid-liquid coexistence below the critical temperature of CO_2, and very limited mutual solubility in the regions of two- and three-phase equilibria. Dodds et al. [5] reviewed the available solubility data for CO_2 in water at temperature below 373 K and attempted to smooth the data with a curve for each isobar, although they recognized that this was difficult because of the discrepancies between different sources. Wilhelm et al. [6] reviewed gas solubility of several gases in water, including CO_2, at temperatures up to 373 K and at pressures below 1 MPa. During the 1990s, Crovetto [7] and Carroll et al. [8] published two important reviews of the solubility data. Following a detailed evaluation of the data, Crovetto [7] found that for this system at temperatures between (273 and 353) K, Henry's constant could be determined with an estimated relative uncertainty of 1 % while, in the wider range of (353 to 600) K, a relative uncertainty of (5 to 10)% was estimated. She concluded that more precise and reliable measurements were called for at temperatures above 353 K. Carroll et al. [8] compiled and critically evaluated the solubility data for CO_2 in water at pressures below 1 MPa from nearly 100 literature sources, and determined an empirical correlation for the Henry's law constant based on what they determined to be the most reliable data. In compiling this correlation, they found several of the data set to be of poor quality and to give large deviations in terms of Henry's constant. Additional data were compiled and tabulated in

the 1996 IUPAC Solubility Series [9]. More recently, the phase behavior of (CO_2 + H_2O) has been reviewed by Spycher et al. [2], Diamond and Akinfiev [10] and Chapoy et al. [11]. Spycher et al. [2] and Chapoy et al. [11] evaluated the available data for both the H_2O-rich and the CO_2-rich phases, although few data for the latter were found. Diamond and Akinfiev [10] evaluated CO_2 solubility in water at pressure as high as 100 MPa and developed an empirical model for the solubility of CO_2 in water. Based on four proposed criteria, they assign different weight factors to the available data sources and rejected entirely 158 of the 520 sources considered. There are also a number of *pVTx* data sets under supercritical conditions available [12-15], and the thermodynamic properties of mixtures of steam and CO_2 have been studied comprehensively by Gallagher et al. [16].

To summarize, a large amount of data are available for the (CO_2 + H_2O) system at temperatures up to 373 K and pressures up to about 10 MPa, although some of the data sets are inconsistent. At higher temperatures and pressures, the available data are fewer and the inconsistencies are greater [10, 11]. But high-temperature high-pressure data are of essential value in the fields of CO_2-EOR and carbon storage. Furthermore, vapor-phase (CO_2 rich) data are much less available compared with liquid-phase data (H_2O rich), [11] but vapor phase data are required for accurate modeling work. Accordingly, the aim of the present work was to investigate the VLE and VLLE of this system at temperatures up to 448 K with pressures approaching 20 MPa.

In this paper, following our previous work on (CO_2 + hydrocarbons) [17], the (CO_2 + H_2O) system is studied as the benchmark for (CO_2 + brine) systems, which are of great interest in CO_2-EOR, carbon storage and geological research. We begin by describing a new analytical apparatus designed and built to study the VLE and VLLE of representative fluids relevant to CO_2-EOR and carbon storage. We further report the results of our measurements on the binary system (CO_2 + H_2O) at temperatures from (298.15 to 448.15) K and pressures between (1.5 and 18) MPa. The new measurements fill the gaps identified in the available data, especially at temperatures higher than 373.15 K and in the high pressure region above 10 MPa. The results are compared comprehensively with the literature published since 1937. The VLE data are modeled by means of the so-called with $\gamma - \phi$ approach in which the vapor phase is described by the Peng-Robinson equation of state (EoS) [18] with classical mixing rules, and the liquid phase is described by an extended form of Henry's law, incorporating both the NRTL solution model [19] and a Poynting correction based on the partial molar volume CO_2 in aqueous solution. The Krichevsky-Kasarnovsky (KK) [20] approach, which is

widely used for modeling the solubility of acid gases in aqueous solvents, is also evaluated for its ability to correlate the data in wide ranges of temperature and pressure. Finally, the solubility model of Duan et al. [21] is tested against our liquid-phase data.

2. Experimental Section

2.1. Apparatus

A circulation-type quasi-static analytical apparatus, shown in Fig. 1, was developed and used in this work. The apparatus included a circulation system, sampling system, sample injection system, and temperature and pressure measuring systems.

The high-pressure vessel, made from Hastelloy C276, was a cylindrical design with an internal volume of approximately 95 mL. The working pressure could be as high as 50 MPa at the maximum working temperature of 473.15 K although, in the present work, it was limited to 18 MPa as detailed below. The vessel was fitted with three sapphire windows located in the back, front, and top of the cell which allowed illumination and observation of the fluids from both in front and, by means of a beam splitter, above. The beam splitter allowed light to pass through the top window, and at the same time permitted observation of the interior for purposes of verifying internal circulation and stirring of the fluids. A photo of the vessel is shown in Fig 1.

The fluid phases were circulated by means of a dual-channel magnetically-coupled pump: one channel drawing vapor from the top of the cell; and the other drawing liquid through a special elbow-pattern probe in the side of the cell. This probe was fitted to a modified swivel joint (SITEC model 729.0305, seen projecting from the vessel in Fig. 1) that could be rotated about the horizontal axis so as to draw in liquid from a variable height within the cell, thereby permitting the study of multiphase systems. The circulation of the vapor and liquid was achieved by reciprocation of a single magnetic piston within the pump cylinder by means of an annular external magnet driven by a pneumatic cylinder. The piston, of o.d. 7.97 mm, had an iron core encased in an outer shell of polyphenylene sulfide (PPS) polymer, chosen to minimize wear on the 8.00 mm i.d. honed bore of the Hastelloy C276 cylinder. Micro-switches located at each end of the range of travel were used to switch solenoid valves that provided air flow to the two ports of the pneumatic cylinder thereby commanding forward and reverse strokes. Each end of the pump cylinder was connected to a tee-piece in the respective flow line, and pairs of gravity-operated check valves ensured uni-directional flow of the gas and liquid phases. In addition to the effects of re-circulation, the contents of the

equilibrium cell were agitated by a magnetic follower placed in the bottom of the vessel. The magnetic follower was driven by a rotating external magnet. The vessel, re-circulation pump and sampling valves were housed within an air oven (Memmert model UFP 600) which was able to maintain the temperature of the vessel constant to within ±0.03 K. The oven was also fitted with two large windows to permit viewing of the cell contents.

The sampling system utilized two high-pressure electro-mechanical sampling valves (ROLSI evolution IV), one located in the suction line of the vapor pump channel and the other in the outflow line of the liquid pump channel. The samplers permit milligram samples to be withdrawn for analysis. In the present case, PPS seals (which are flexible and robust, and exhibit extremely low water absorption) were used in the sampling valves but, for leak-free operation, these were limited to a maximum pressure of 18 MPa. The two sampling valves were connected in series with the carrier gas flow to the gas chromatograph by means of heated transfer lines. The sampling valves and transfer line were operated at a temperature of 473 K thereby ensuring rapid vaporization of the volatile components of a liquid sample. Compositional analysis was performed by on-line gas chromatography (Agilent 7890A GC system). The GC was equipped with a split/spitless injector, an HP-PLOT-Q capillary column (length 30 m, o.d. 0.32mm, 20 μm film thickness) and a thermal conductivity detector. The carrier gas flow rate, oven temperature, and detector temperature of the GC were optimized to give the best separation performance for both vapor and liquid samples.

Fluids were injected from a three-cylinder syringe pump system (Quizix model Q5310-HC-A-GH-S, Vindum Engineering) connected in parallel with the inlet port. The pumps had wetted parts of Hastelloy C276 and ceramic, with seals of ultra-high molecular weight polyethylene. One syringe was fitted with a cooling jacket and maintained at a temperature of approximately 278 K by means of a circulating chiller; this channel was used to pump liquefied CO_2. A second channel was used to pump water and, in the present work, the third channel was unused. A pneumatically-operated valve (model CV-420, Vindum Engineering) was fitted in the inlet line immediately before the vessel and used to isolate the system from the pumps during equilibration stages. The system was protected from over pressurization by means of a rupture-disc safety head connected directly to one port of the equilibrium cell.

The experimental temperature was measured by means of a platinum resistance thermometer (PT100, Sensing Devices Ltd) located in a thermowell bored in the wall of the equilibrium cell. The resistance of this thermometer was measured with a data acquisition/switch unit (model 34970A, Agilent Technologies) interfaced with the control computer. The pressure was measured with a transducer with a full-scale range of 50 MPa

(model Super TJE, Honeywell) connected in the circulation loop. The voltage output of the pressure transducer was digitized and displayed by a transducer readout unit (model E725, RDP Electronics Ltd) also interfaced to the control computer. The circulation pump and the inlet valve were also activated through relays in the data acquisition/switch unit under computer control.

2.2. Calibration

The platinum resistance temperature was calibrated on the International Temperature Scale of 1990 at the temperature of the triple point of water and by comparison in a constant-temperature bath with a standard platinum resistance thermometer (SPRT). The resistance of the SPRT was measured with a high-precision thermometry bridge (model 1594A super thermometer, Fluke). The overall standard uncertainty of the temperature measurements was estimated to be ±0.04 K, including the uncertainty of the temperature sensor itself, calibration uncertainties and the effects of temperature fluctuations in the oven.

The pressure transducer was calibrated against a high pressure pneumatic controller/calibrator (model PPCH-G, Fluke) over the full pressure range of 50 MPa. Considering the observed fluctuations and the uncertainties in the transducer calibration, the total pressure standard measurement uncertainty was found to be 0.04 % of reading.

To permit accurate calibration of the GC, a four-port sampling valve (model ED2CI4UW1, Vici AG International) with an internal sample loop volume of 1 μL was connected in series with the two Rolsi samplers. Different amounts of pure CO_2 could be injected for GC analysis by varying the loop filling pressure while, in separate injections, different amounts of water could be analyzed by filling the loop with mixtures of water and tetrahydrofuran having various known compositions. The loop filling pressure and temperature were monitored so that the thermodynamic state of the calibration fluid was precisely known. By assuming a loop volume of 1μL, absolute calibration of the GC could be accomplished leading to response factors relating peak area to molar amount of each component. In fact, the loop volume was not known accurately but this factor cancels out in the determination of a mixture composition. The GC calibration results for CO_2 and water are shown in Fig. 2. Near-perfect linear calibration lines were found in both cases, thus, the uncertainty of composition measurement is mainly from the deviations of individual sample injections and GC analysis. The average standard uncertainties were found to be 3×10^{-4} and 8×10^{-4} for the mole fractions in liquid and vapor phases respectively.

2.3. Experimental Procedure and Results

Pure de-ionized water with electrical resistivity > 18 MΩ·cm was used; this was produced by a Millipore water purification unit. The water was degassed under vacuum immediately prior to use. The carbon dioxide was supplied by BOC with a claimed mole-fraction purity of 99.995%.

The system was first evacuated to a pressure of approximately 1 kPa using a two-stage diaphragm pump, and then flushed with CO_2 and evacuated again to ensure removal of impurities. A selected amount of water was then charged into the cell. With the temperature controlled at the desired value, CO_2 was charged into the vessel until the desired initial pressure was reached. The system was equilibrated under the action of the recirculation pump and the magnetic stirrer before sampling of the phases commenced.

The equilibrium state was first judged from constancy of the measured pressure, and then by monitoring the reproducibility of vapor and liquid sample compositions. For all the isotherms studied, an equilibrium condition was reached within approximately 2 hours. Once equilibrium was reached, samples of liquid and vapor were taken and transferred to the on-line GC for analysis. Typical sample sizes were around 35 μmol for the liquid phase and 15 μmol for the vapor phase. Approximately 10 samples of each phase with good composition reproducibility were taken for analysis to give final mean results. The temperature and pressure were measured before, during and after the sampling and mean values taken.

A further amount of CO_2 was then charged into the vessel to reach another equilibrium state at a higher pressure, and the procedure was repeated for the other isotherms.

The experimental data are listed in Table 1 together with the standard uncertainty of the mole fractions. The results are illustrated in Fig 3 to 9 for all 7 isotherms measured between (298.15 and 448.15) K. At T = 298.15 K, VLLE data were measured at a pressure of 6.391 MPa and, above this pressure, LLE data were measured.

3. Modeling

Typically, thermodynamic models based on the symmetric $\phi-\phi$ approach and the asymmetric $\gamma-\phi$ approach could be applied to model the phase behavior of (CO_2 + H_2O). Models based on these two approaches can be found in the work of King et al. [22], Valtz et al. [23] and Paulus and Penoncello [24]. Since we wish to model also (CO_2 + brine) mixtures, the $\gamma-\phi$ approach is more favorable because activity coefficients are required for chemical

equilibrium and mineral speciation calculations.

The $\gamma-\phi$ approach is known for its ability to describe both the vapor and liquid phases by representing the liquid phase with a solution model and the vapor phase with an equation of state. It is also the basis of the Krichevsky-Kasarnovsky (KK) approach, which is widely used for modeling the solubility of acid gas in aqueous solvents. It should be noted that the KK approach can only describe the solubility of the gas solute in the liquid phase, and can be seen as a simplified $\gamma-\phi$ approach.

In this work, we modeled our data for (CO_2 + H_2O) primarily with the $\gamma-\phi$ approach, considering both the liquid and vapor compositions. We further investigated the KK approach to model the liquid phase data. Duan's correlation model, which is widely used for modeling CO_2 solubility in water and brines, is also applied here for comparison purposes.

3.1. $\gamma-\phi$ approach

In the $\gamma-\phi$ approach, an extended form of Henry's law is applied to describe the fugacity of component 1 (CO_2) in the liquid phase, under the assumption that the partial molar volume is independent of both pressure and composition. Thus the equality of fugacity for component 1 is expressed as:

$$y_1\hat{\phi}_1 p = x_1\gamma_1^* H_{12}\exp\left[\bar{V}_1^{\infty}\left(p-p^{\mathrm{ref}}\right)/RT\right] \quad (1)$$

Here, p is the system pressure, T is the system temperature, $\hat{\phi}_1$ is the fugacity coefficient of CO_2 in the vapor phase, y_1 and x_1 are the vapor and liquid phase mole fractions of CO_2, respectively, γ_1^* is the activity coefficient of CO_2 (normalized to unity at infinite dilution), p^{ref} is the reference pressure, H_{12} is the Henry's law constant for CO_2 in aqueous solution, and $\bar{V}_1^{\infty}$ is the partial molar volume of CO_2 at infinite dilution in aqueous solution. In this work, $\bar{V}_1^{\infty}$ was obtained from the correlation of Sedlbauer et al [25] and p^{ref} was taken as the vapor pressure of pure H_2O at temperature T.

For component 2 (H_2O), in the asymmetric approach, the liquid phase standard state fugacity is the fugacity of the pure saturated solvent at the given temperature. The equality of fugacity is expressed as:

$$y_2\hat{\phi}_2 p = x_2\gamma_2\phi_2^{\mathrm{sat}} p_2^{\mathrm{sat}}\exp\left[V_2^{\mathrm{sat}}\left(p-p^{\mathrm{ref}}\right)/RT\right] \quad (2)$$

where y_2 and x_2 are the vapor and liquid phase mole fractions of H_2O, respectively, $\hat{\phi}_2$ is the fugacity coefficient of H_2O in the vapor phase, γ_2 is the activity coefficient of H_2O (normalized to unity for pure water), and ϕ_2^{sat}, p_2^{sat} and V_2^{sat} are the fugacity coefficient, vapor pressure and liquid molar volume for pure saturated water, respectively; these values are taken from REFPROP 9.0 [26]. From the definition above, $p^{ref} = p_2^{sat}$.

The Peng-Robinson equation of state (PR EoS) with classical mixing rules was used to model the vapor phase non-ideality. The PR EoS is known for its ability to describe the vapor pressure of both nonpolar and polar compounds. For a pure compound, it is expressed as:

$$p = \frac{RT}{V-b} - \frac{a(T)}{V(V+b)+b(V-b)} \tag{3}$$

where p, V and T are pressure, molar volume, and temperature, R is the universal gas constant, and a and b are the energy and co-volume parameters given as follows:

$$a = 0.457235(RT_c)^2\alpha(T)/p_c \tag{4}$$

$$\alpha(T) = \left[1+(0.37464+1.54226\omega-0.26992\omega^2)(1-(T/T_c)^{0.5})\right]^2 \tag{5}$$

$$b = 0.077796RT_c/p_c \tag{6}$$

Here, p_c, T_c and ω are the critical pressure, critical temperature and acentric factor for each pure compound; the values applicable to CO_2 and H_2O, taken from REFPROP version 9.0 [26], are given in Table 2. The classical mixing rules used to apply the PR EoS to mixtures are given as:

$$a = \sum_i \sum_j x_i x_j (1-k_{ij})\sqrt{a_i a_j} \tag{7}$$

$$b = \sum_i \sum_j x_i x_j (b_i + b_j)/2 \tag{8}$$

where a_i and b_i are the energy and co-volume parameters for pure component i and k_{ij} is the binary interaction parameter between components i and j.

In the literature, γ_1^* and γ_2 are often taken to be unity on the grounds that the two components have very limited mutual solubilities [2, 22]. However, we argue that, whereas the assumption relating to H_2O may be acceptable, variation of the activity coefficient of CO_2

cannot be ignored. In this work, the activity coefficients of CO_2 (1) and H_2O (2) are represented with the NRTL solution model [19] in terms of which:

$$\ln \gamma_1^* = x_2^2 \left[\tau_{21} \left(\frac{G_{21}}{x_1 + x_2 G_{21}} \right)^2 + \frac{\tau_{12} G_{12}}{\left(x_2 + x_1 G_{12} \right)^2} \right] - \left(\tau_{21} + \tau_{12} G_{12} \right) \tag{9}$$

$$\ln \gamma_2 = x_1^2 \left[\tau_{12} \left(\frac{G_{12}}{x_2 + x_1 G_{12}} \right)^2 + \frac{\tau_{21} G_{21}}{\left(x_1 + x_2 G_{21} \right)^2} \right] \tag{10}$$

with

$$G_{12} = \exp\left(-\alpha_{12} \tau_{12} \right) \tag{11}$$

where τ_{12} and τ_{21} are the local binary interaction parameters, α_{12} is the non-randomness parameter which is taken here to be 0.3 considering that this is a polar-nonpolar mixture [27].

The binary interaction parameter k_{12} was found to be temperature dependent, and a linear function of inverse temperature correlated the parameter very well:

$$k_{12} = A + B(T_0 / T) \tag{12}$$

where T_0 = 298.15 K. For the Henry's law constant H_{12}, which is also temperature dependent, the following correlation function was applied:

$$\ln(H_{12} / \text{MPa}) = C_0 + C_1 \left(T_0 / T \right) + C_2 \left(T_0 / T \right)^2 + C_3 \left(T_0 / T \right)^3 \tag{13}$$

where C_i (i = 0 to 3) were adjustable parameters. A plot for Henry's law constant H_{12} is shown in Fig. 10. Finally, it was found that the NRTL interaction parameters τ_{12} and τ_{21} could be described with the following equation:

$$\tau_{ij} = D_{ij} + \frac{E_{ij}}{T} + F_{ij} \left[\frac{T_0 - T}{T} + \ln\left(\frac{T}{T_0} \right) \right] , \tag{14}$$

where D_{ij}, E_{ij} and F_{ij} are the parameters. The 12 parameters appearing in Eqs. 12 to 14 were optimized in isothermal bubble point calculations, considering simultaneously all isotherms, coupled with the Levenberg-Marquardt optimization algorithm [28], using the following objective function:

$$\Delta = \sum_{i=1}^{N} \left(\frac{p_i^{\text{exp}} - p_i^{\text{cal}}}{p_i^{\text{exp}}} \right)^2 . \tag{15}$$

Here, p_i^{exp} and p_i^{cal} are the experimental and calculated bubble pressure at the i^{th} state point, having specified T and x, and N is the number of data points. The final parameters values are listed in table 3 and, in table 4, we give the average absolute deviations (AAD) of pressure and vapor phase mole fraction for each isotherm.

3.2. Krichevsky-Kasarnovsky (KK) approach

The Krichevsky-Kasarnovsky (KK) approach [20] is based on a simplification of Eq. (1) in which the activity coefficient of the solute is set to unity. The KK equation is usually expressed in the form:

$$\ln\left(\frac{\hat{f}_1^{V}}{x_1}\right) = \ln H_{12} + \frac{\overline{V}_1^{\infty}(p - p^{ref})}{RT} \qquad (16)$$

where $\hat{f}_1^{V}$ is the fugacity of CO_2 in the vapor phase. Since, in this work, we measured the coexisting vapor phase composition at each pressure, the fugacity was calculated from the PR EoS with classical mixing rules applied at the experimental temperature, pressure and vapor phase composition. The binary interaction parameter k_{ij} was obtained from Eq. 12.

The KK equation implies that the left part of Eq. 16 has a linear relation with pressure at given temperature, with $\ln H_{12}$ as the intercept. For each isotherm, the Henry's law constant H_{12} and partial molar volume of CO_2 at infinite dilution $\overline{V}_1^{\infty}$ are listed in Table 5.

4. Discussion

The (CO_2 + H_2O) mixture exhibits type III phase behavior according to the classification of Scott and Konynenburg [4]. As shown by Diamond and Akinfiev [10], the vapor-liquid-liquid three phase line is very close to the saturated vapor pressure of pure CO_2. In this work, we measured the VLLE point at T = 298.15 K. Three LLE data points were measured at T = 298.15 K and higher pressures. All the other measurements were of VLE states.

The results are shown in comparison with literature data in Fig. 3 to Fig. 9. As discussed earlier, although there are relatively large amounts of published data available, significant disagreement exists between different sources. In the evaluation work of Carroll et al. [8] and Diamond and Akinfiev [10], several literature sources were recommended as reliable. For the liquid phase, the following sources were highly rated: at T = 323.15 K, the data of Zawisza and Malesinska [29] and Bamberger et al. [30]; at T = 348.15 K, the data of Zawisza and

Malesinska [29]; at T = 373.15 K, the data of Zawisza and Malesinska [29], Wiebe and Gaddy [31] and Müller et al. [32]; at T = 398.15 K, the data of Zawisza and Malesinska [29] and Müller et al.[32]; and at T = 423.15 K and T = 448.15 K, the data of Zawisza and Malesinska [29]. As can be seen from the *p-x* diagrams, our liquid phase results are in good agreement with these data sets. Zawisza and Malesinska [29] studied most of the isotherms measured in the present work, although their data are at lower pressures (below 5.0 MPa), while those of Bamberger et al. [30] and King et al. [22] are at high pressures, but at low temperatures (below 363 K). There are several other highly rated data sets, including those of Davies et al. [33], Perez and Sandall [34], and Won et al. [35] but these pertain to different isotherms and are restricted to low pressures (around 1.0 MPa).

For the vapor phase results, there are fewer data available with which to compare and no comprehensive evaluation has been published. Since the liquid phase data of Bamberger et al., [30] Müller et al.[32], and Zawisza and Malesinska [29] are recommended, their vapor phase data, where available, are compared with our results. As can be seen from the *p-y* diagrams, our data again show good consistency with these literature sources. At temperatures higher than 373.15 K, only limited vapor phase data are available and, for example, at T = (373.15, 423.15, and 448.15) K, we have resorted to comparison with data sets at slightly different temperatures. Also as shown in the *p-y* diagrams, at temperatures below 373.15 K, the vapor phase mole fraction of H_2O at first decreases rapidly with increasing pressure, and then increases while, at $T \geq 373.15$ K, the mole fraction of H_2O decreases with increasing pressure towards a nearly constant limiting value at high pressures. So our new measurements fill gaps in the available accurate and high-quality liquid phase data at high temperature and high pressure, while also providing valuable new vapor-phase data.

As can be seen from Table 1 and Table 4, our experimental data can be well represented using the $\gamma - \phi$ approach and generalized model parameters, with an overall AAD of 2.3% for pressure; the average vapor phase composition deviation is 0.011. The calculated results are shown in Fig. 11 and 12 together with the experimental results. The *p-x* data are especially well represented, while the worst deviations are found for the *p-y* data at low temperatures and high pressures. An analysis in which the objective function was extended to incorporate deviations of the vapor-phase mole fraction did not lead to a significantly better overall representation of the data.

Our correlation (Eq. 13) for the Henry's law constant H_{21} is compared in Fig. 10 with the correlation reported by Carroll et al. [8] and with values from Zawisza and Malesinska [29].

As stated by Carroll et al. [6], their correlation for H_{21} is valid for $273 \leq T/\mathrm{K} \leq 433$ and was based on experimental data at pressures below 1.0 MPa. Zawisza and Malesinska [16] evaluated the Henry's law constant both from their own experimental results and from selected literature data. It can be seen that the correlation of Carroll et al. [8] shows larger deviations compared with ours and most of the reported literature values.

As discussed in section 3.1, while the activity coefficients of H_2O can be reasonably set to unity, the activity coefficients of CO_2 depart significantly from unity as system pressure increases. Examples results calculated from the asymmetric model are shown in Fig 13 for T = (323.15, 373.15 and 423.15) K. Here we plot the activity coefficients, γ_1^* of CO_2 and γ_2 of H_2O, in the saturated liquid phase as a function of the corresponding bubble-point pressure at given temperature. It can be seen that γ_1^* departs significantly from unity but that $\gamma_2 \approx 1$ in all cases.

The analysis according to the KK approach is illustrated in Fig. 14 where we plot $\ln\left(\hat{f}_1^{\mathrm{V}}/x_1\right)$ against p. At temperatures below 373.15 K, the KK approach gives a reasonably good representation of our data but, at higher temperatures, the KK approach either fails to fit the data or gives an unphysical negative slope (i.e. a negative partial molar volume for CO_2). Similar behavior was found and discussed by Carroll and Mather [36]. They stated that the KK approach can be used for temperatures below 373.15 K, but that activity coefficients could not be neglected at higher temperatures. The results based on the KK approach are summarized in Table 5 for each isotherm, while the calculated Henry's law constants are also shown in Fig. 10. We note that, although the KK approach fails at high temperature, the Henry's law constants obtained are still close to the values determined in the $\gamma - \phi$ approach.

The solubility model of Duan et al. [21] was developed for (CO_2 + water) and (CO_2 + brine) systems and it is interesting to compare it with the present results. This comparison is illustrated along four isotherms in Fig. 15. We see that the model represents our data rather well on the isotherms at $T \leq 423.15$ K; however, at T = 448.15 K, the model disagrees significantly with our data, although Duan et al. stated that their model is valid at temperatures up to 533 K. The apparent deterioration in the accuracy of the model at high temperatures may simply reflect the lack of reliable data in that region.

5. Conclusions

The phase behavior of (CO_2 + H_2O) was measured at temperature from 298.15 K to 448.15 K, and at pressures up to 18 MPa. The experimental results are compared comprehensively with literature data and found to agree with those literature sources identified in earlier reviews as being of the highest reliability. Our results fill key gaps in terms of accurate and high-quality data at high temperature and pressure, and pave the way for measurements on (CO_2 + brine) systems. The results are modeled accurately with a $\gamma - \phi$ approach incorporating the Peng-Robinson EoS with the classical mixing rules for the vapor phase, and an extended form of Henry's law with the NRTL solution model and a Poynting correction for the liquid phase. The Krichevsky-Kasarnovsky (KK) (simplified $\gamma - \phi$ approach) was also studied as well as the empirical correlation of Duan et al.. Both were found to have significant deficiencies for this system.

Nomenclature

a	EoS energy parameter
AAD	average absolute deviation
A, B	parameter in Eq. 12
b	covolume parameter
C_0, C_1, C_2, C_3	parameters in Eq. 13
D, E, F	parameters in Eq. 14
f	fugacity coefficient
H	Henry's law constant
G	NRTL model parameter
k_{ij}	binary interaction parameter in the classical mixing rules
N	number of data points
p	pressure
R	universal gas constant
T	temperature

V	molar volume
x	molar fraction in the liquid phase
y	molar fraction in the vapor phase

Greek letters

α	non-randomness parameter
$\alpha(T)$	EoS temperature dependent function
ω	acentric factor
γ	activity coefficient
τ	binary interaction parameter for NRTL model
Δ	deviations, objective function
*	asymmetric reference state

Subscripts

c	critical point
i, j	component *i, j* and data point *i*

Superscripts

cal	calculated value
exp	experimental value
sat	saturated state
ref	reference state
L	liquid phase
V	vapor phase
∞	infinite dilution

Acknowledgements

We gratefully acknowledge the funding of QCCSRC provided jointly by Qatar Petroleum, Shell, and the Qatar Science & Technology Park.

References

[1] DECHEMA Database, Frankfurt, Germany.
[2] N. Spycher, K. Pruess, J. Ennis-King, CO_2-H_2O mixtures in the geological sequestration of CO_2. I. Assessment and calculation of mutual solubilities from 12 to 100 °C and up to 600 bar, Geochimica et Cosmochimica Acta 67 (2003) 3015-3031.
[3] R.L. Scott, P.H. van Konynenburg, Static properties of solutions. van der Waals and related models for hydrocarbon mixtures, Discussions of the Faraday Society 49 (1970) 87-97.
[4] R.L. Scott, P.H. van Konynenburg, Critical lines and phase equilibria in binary van der Waals mixtures, Philosophical Transactions of the Royal Society of London. Series A 298 (1980) 495-540.
[5] W.S. Dodds, L.F. Stutzman, B.J. Sollami, Carbon dioxide solubility in water, Industrial & Engineering Chemistry Chemical & Engineering Data Series 1 (1956) 92-95.
[6] E. Wilhelm, R. Battino, R.J. Wilcock, Low-pressure solubility of gases in liquid water, Chemical Reviews 77 (1977) 219-262.
[7] R. Crovetto, Evaluation of solubility data of the system CO_2-H_2O from 273 K to the critical point of water, Journal of Physical and Chemical Reference Data 20 (1991) 575-589.
[8] J.J. Carroll, J.D. Slupsky, A.E. Mather, The solubility of carbon dioxide in water at low pressure, Journal of Physical and Chemical Reference Data 20 (1991) 1201-1209.
[9] IUPAC Solubility Data Series, vol. 62.
[10] L.W. Diamond, N.N. Akinfiev, Solubility of CO_2 in water from −1.5 to 100 °C and from 0.1 to 100 MPa: Evaluation of literature data and thermodynamic modelling, Fluid Phase Equilibria 208 (2003) 265-290.
[11] A. Chapoy, A.H. Mohammadi, A. Chareton, B. Tohidi, D. Richon, Measurement and modeling of gas solubility and literature review of the properties for the carbon dioxide-water system, Industrial & Engineering Chemistry Research 43 (2004) 1794-1802.
[12] S.D. Malinin, Thermodynamics of the H_2O-CO_2 system., Geochemistry International 11 (1974) 1060-1085.
[13] E.U. Franck, K. Todheide, Thermal properties of supercritical mixtures of carbon dioxide and water up to 750°C and 2000 atmospheres, Zeitschrift für Physikalische Chemie NeueFolge 22 (1959) 232-245.
[14] H.J. Greenwood, The compressibility of gaseous mixtures of carbon dioxide and water between 0 and 500 bars pressure and 450°C and 850°C, American Journal of Science 267 (1969) 191-208.
[15] H.J. Greenwood, Thermodynamic properties of gaseous mixures of H_2O and CO_2 between 450 °C and 800 °C and 0 to 500 bars, American Journal of Science 273 (1973) 561-571.
[16] J.S. Gallagher, R. Crovetto, J. Sengers, The thermodynamic behavior of the CO_2-H_2O system from 400 to 1000 K, upto 100 MPa and 30% mole fraction of CO_2, Journal of Physical and Chemical Reference Data 22 (1993) 431-513.
[17] S.X. Hou, G.C. Maitland, J.P.M. Trusler, An analytical apparatus for phase equilibria studies of representative reservoir, 21st IUPAC International Conference on Chemical Thermodynamics, Ibaraki, Japan, August 1-6 (2010).
[18] D.Y. Peng, D.B. Robinson, A new two-constant equation of state, Industrial & Engineering Chemistry Fundamentals 15 (1976) 59-64.
[19] H. Renon, J.M. Prausnitz, Local compositions in thermodynamic excess functions for liquid mixtures, AIChE Journal 14 (1968) 135-144.
[20] I.R. Krichevsky, J.S. Kasarnovsky, Thermodynamical calculations of solubilities of nitrogen and hydrogen in water at high pressures, Journal of the American Chemical Society 57 (1935) 2168-2171.
[21] Z. Duan, R. Sun, C. Zhu, I.M. Chou, An improved model for the calculation of CO_2 solubility in aqueous solutions containing Na^+, K^+, Ca^{2+}, Mg^{2+}, Cl^-, and SO_4^{2-}, Marine Chemistry 98 (2006) 131-139.
[22] M.B. King, A. Mubarak, J.D. Kim, T.R. Bott, The mutual solubilities of water with supercritical and liquid carbon dioxides, The Journal of Supercritical Fluids 5 (1992) 296-302.
[23] A. Valtz, A. Chapoy, C. Coquelet, P. Paricaud, D. Richon, Vapour-liquid equilibria in the carbon dioxide–water system, measurement and modelling from 278.2 to 318.2 K, Fluid Phase Equilibria 226 (2004) 333-344.
[24] M. Paulus, S. Penoncello, Correlation for the carbon dioxide and water mixture based on the Lemmon–Jacobsen mixture model and the Peng-Robinson equation of state, International Journal of Thermophysics 27 (2006) 1373-1386.
[25] J. Sedlbauer, J.P. O'Connell, R.H. Wood, A new equation of state for correlation and prediction of standard molal thermodynamic properties of aqueous species at high temperatures and pressures, Chemical Geology 163 (2000) 43-63.
[26] E.W. Lemmon, M.L. Huber, M.O. McLinden, Reference Fluid Thermodynamic and Transport Properties (REFPROP), NIST Standard Reference Database 23, Version 9.0, Physical and Chemical Properties Division, National Institute of Standards and Technology, Gaithersburg, MD, (2010).
[27] J.M. Prausnitz, R.N. Lichtenthaler, E. Gomes de Azevedo, Molecular Thermodynamics of Fluid-Phase Equilibria (3rd edition), Prentice Hall PTR (1999).
[28] J.L. Kuester, J.H. Mize, Optimization Techniques with Fortran, McGraw-Hill: New York (1973).

[29] A. Zawisza, B. Malesinska, Solubility of carbon dioxide in liquid water and of water in gaseous carbon dioxide in the range 0.2-5 MPa and at temperatures up to 473 K, Journal of Chemical & Engineering Data 26 (1981) 388-391.
[30] A. Bamberger, G. Sieder, G. Maurer, High-pressure (vapor+liquid) equilibrium in binary mixtures of (carbon dioxide+water or acetic acid) at temperatures from 313 to 353 K, J. Supercrit. Fluids 17 (2000) 97-110.
[31] R. Wiebe, V.L. Gaddy, The solubility in water of carbon dioxide at 50, 75 and 100°C, at pressures to 700 atmospheres, Journal of the American Chemical Society 61 (1939) 315-318.
[32] G. Müller, Experimental study of the vapor-liquid equilibrium in the system ammonia-carbon dioxide-water from 100 to 200 °C at pressures up to 90 bar, Thesis, Univ. Kaiserslautern (1983).
[33] G.A. Davies, A.B. Ponter, K. Craine, The diffusion of carbon dioxide in organic liquids, The Canadian Journal of Chemical Engineering 45 (1967) 372-376.
[34] J.F. Perez, O.C. Sandall, Carbon dioxide solubility in aqueous carbopol solutions at 24°C, 30 °C, and 35 °C, Journal of Chemical & Engineering Data 19 (1974) 51-53.
[35] Y.S. Won, D.K. Chung, A.F. Mills, Density, viscosity, surface tension, and carbon dioxide solubility and diffusivity of methanol, ethanol, aqueous propanol, and aqueous ethylene glycol at 25 °C, Journal of Chemical & Engineering Data 26 (1981) 140-141.
[36] J.J. Carroll, A.E. Mather, The system carbon dioxide-water and the Krichevsky-Kasarnovsky equation, Journal of Solution Chemistry 21 (1992) 607-621.
[37] C.E.P.S. Campos, H.G.D.A. Villardi, F.L.P. Pessoa, A.M.C. Uller, Solubility of carbon dioxide in water and hexadecane: Experimental measurement and thermodynamic modeling, Journal of Chemical & Engineering Data 54 (2009) 2881-2886.
[38] I. Dalmolin, E. Skovroinski, A. Biasi, M.L. Corazza, C. Dariva, J.V. Oliveira, Solubility of carbon dioxide in binary and ternary mixtures with ethanol and water, Fluid Phase Equilibria 245 (2006) 193-200.
[39] T. Nakayama, H. Sagara, K. Arai, S. Saito, High pressure liquid-liquid equilibria for the system of water, ethanol and 1,1-difluoroethane at 323.2 K, Fluid Phase Equilibria 38 (1987) 109-127.
[40] R. Vilcu, I. Gainar, Loslichkeit der gase unter druck in flussigkeiten. I. Das system kohlendioxid-wasser, Revue Roumaine De Chimie 12 (1967) 181-189.
[41] Y.D. Zelvenskii, The solubility of carbon dioxide under pressure, Journal of Chemical Industry 14 (1937) 1250-1257.
[42] R. Wiebe, V.L. Gaddy, Vapor phase composition of carbon dioxide-water mixtures at various temperatures and at pressures to 700 atmospheres, Journal of the American Chemical Society 63 (1941) 475-477.
[43] C.R. Coan, A.D. King, Solubility of water in compressed carbon dioxide, nitrous oxide, and ethane. Evidence for hydration of carbon dioxide and nitrous oxide in the gas phase, Journal of the American Chemical Society 93 (1971) 1857-1862.
[44] P.C. Gillespie, G.M. Wilson, Vapor-liquid and liquid-liquid equilibria: Water-methane, water-carbon dioxide, water-hydrogen sulfide, water-n-pentane, water-methane-n-pentane, GPA Research Report RR-48 (1982) 1-73.
[45] H. Teng, A. Yamasaki, M.K. Chun, H. Lee, Solubility of liquid co_2 in water at temperatures from 278 K to 293 K and pressures from 6.44 MPa to 29.49 MPa and densities of the corresponding aqueous solutions, The Journal of Chemical Thermodynamics 29 (1997) 1301-1310.
[46] R. D'Souza, J.R. Patrick, A.S. Teja, High pressure phase equilibria in the carbon dioxide - n-hexadecane and carbon dioxide-water systems, The Canadian Journal of Chemical Engineering 66 (1988) 319-323.
[47] J.A. Briones, J.C. Mullins, M.C. Thies, B.U. Kim, Ternary phase equilibria for acetic acid-water mixtures with supercritical carbon dioxide, Fluid Phase Equilibria 36 (1987) 235-246.
[48] S. Bando, F. Takemura, M. Nishio, E. Hihara, M. Akai, Solubility of CO_2 in aqueous solutions of NaCl at (30 to 60) °C and (10 to 20) MPa, Journal of Chemical & Engineering Data 48 (2003) 576-579.
[49] K. Fischer, M. Petri, J. Chen, O. Noll, J. Gmehling, Unpublished data, (1995).
[50] R.D. Smith, H.R. Udseth, B.W. Wright, Micro-scale methods for characterization of supercritical fluid extraction and fractionation processes, Process Technology Proceedings 3 (1985) 191-223.
[51] I.P. Sidorov, Y.S. Kazarnovskii, A.M. Goldman, The solubility of water in compressed gases, Tr. Gos. Nauchno Issled. Proektn. Inst. Azotn. Promst. Prod. Org. Sin. 1 (1953) 48-67.
[52] T. Sako, T. Sugeta, N. Nakazawa, T. Okubo, M. Sato, T. Taguchi, T. Hiaki, Phase equilibrium study of extraction and concentration of furfural produced in reactor using supercritical carbon dioxide, Journal of Chemical Engineering Japan 24 (1991) 449-455.
[53] J. Kiepe, S. Horstmann, K. Fischer, J. Gmehling, Experimental determination and prediction of gas solubility data for CO_2 + H_2O mixtures containing NaCl or KCl at temperatures between 313 and 393 K and pressures up to 10 mpa, Industrial & Engineering Chemistry Research 41 (2002) 4393-4398.
[54] C.F. Prutton, R.L. Savage, The solubility of carbon dioxide in calcium chloride-water solutions at 75, 100, 120°C and high pressures, Journal of the American Chemical Society 67 (1945) 1550-1554.
[55] J.A. Nighswander, N. Kalogerakis, A.K. Mehrotra, Solubilities of carbon dioxide in water and 1 wt. %

sodium chloride solution at pressures up to 10 MPa and temperatures from 80 to 200 °C, Journal of Chemical & Engineering Data 34 (1989) 355-360.
[56] S. Takenouchi, G.C. Kennedy, The solubility of carbon dioxide in nacl solutions at high temperatures and pressures, American Journal of Science 263 (1965) 445-454.
[57] G. Brunner, Phase equilibria in presence of compressed gases and their relevance to the separation of low-volatile substances, Dissertation, University Erlangen-Nuernberg (1978).
[58] S. Takenouchi, G.C. Kennedy, The binary system H_2O-CO_2 at high temperatures and pressures, American Journal of Science 262 (1964) 1055-1074.

Table 1.
Experimental and calculated results for the CO_2 (1) + H_2O (2) system.[a]

T (K)	p^{exp} (MPa)	x_1^{exp}		y_1^{exp}		$x'_1{}^{exp}$		y_1^{cal}	p^{cal} (MPa)
298.15	1.666	0.00887	± 0.00016	0.99732	± 0.00025			0.99746	1.646
298.15	3.258	0.01540	± 0.00021	0.99840	± 0.00005			0.99820	3.124
298.15	6.391	0.02484	± 0.00031	0.99806	± 0.00007	0.99735	± 0.00008	0.99700	6.471
298.15	10.183	0.02630	± 0.00062			0.99551	± 0.00013		
298.15	13.434	0.02782	± 0.00056			0.99442	± 0.00021		
298.15	17.551	0.02944	± 0.00052			0.99323	± 0.00015		
323.15	1.089	0.00333	± 0.00011	0.97189	± 0.00050			0.98626	1.021
323.15	2.980	0.00901	± 0.00008	0.99493	± 0.00012			0.99380	2.984
323.15	7.406	0.01829	± 0.00035	0.99650	± 0.00024			0.99389	7.746
323.15	10.021	0.02054	± 0.00044	0.99597	± 0.00005			0.98635	10.272
323.15	12.973	0.02141	± 0.00134	0.99467	± 0.00007			0.97413	12.598
323.15	17.533	0.02255	± 0.00047	0.99386	± 0.00003			0.95958	17.537
348.15	1.101	0.00222	± 0.00008	0.96868	± 0.00061			0.95820	1.016
348.15	2.921	0.00608	± 0.00022	0.98578	± 0.00021			0.98198	2.883
348.15	7.123	0.01267	± 0.00053	0.99155	± 0.00013			0.98752	6.947
348.15	10.167	0.01593	± 0.00021	0.99195	± 0.00009			0.98603	9.870
348.15	13.282	0.01856	± 0.00020	0.99164	± 0.00007			0.97869	13.635
348.15	16.918	0.01993	± 0.00023	0.99004	± 0.00009			0.96878	17.006
373.15	1.107	0.00169	± 0.00005	0.91198	± 0.00079			0.89608	1.049
373.15	2.426	0.00390	± 0.00012	0.95309	± 0.00027			0.94842	2.361
373.15	7.088	0.01085	± 0.00026	0.97898	± 0.00011			0.97349	7.314
373.15	10.235	0.01365	± 0.00039	0.98253	± 0.00008			0.97415	9.936
373.15	13.352	0.01626	± 0.00039	0.98325	± 0.00009			0.97160	13.053
373.15	17.070	0.01872	± 0.00047	0.98288	± 0.00011			0.96436	17.154
398.15	1.158	0.00142	± 0.00029	0.78688	± 0.00163			0.78681	1.150
398.15	3.176	0.00444	± 0.00010	0.91471	± 0.00095			0.91198	3.215
398.15	7.321	0.01005	± 0.00031	0.95542	± 0.00048			0.94843	7.601
398.15	9.984	0.01308	± 0.00010	0.96440	± 0.00034			0.95284	10.431
398.15	13.456	0.01573	± 0.00024	0.96637	± 0.0008			0.95290	13.340
398.15	17.435	0.01857	± 0.00029	0.96910	± 0.00030			0.94915	17.171
423.15	1.428	0.00127	± 0.00002	0.65360	± 0.00050			0.63334	1.352
423.15	2.987	0.00348	± 0.00004	0.81073	± 0.00117			0.81497	2.935
423.15	7.197	0.00870	± 0.00021	0.90548	± 0.00069			0.90108	6.984
423.15	10.014	0.01231	± 0.00024	0.92501	± 0.00049			0.91705	10.147
423.15	13.418	0.01557	± 0.00023	0.93632	± 0.00088			0.92253	13.370
423.15	17.355	0.01905	± 0.00022	0.94339	± 0.00055			0.92262	17.368
448.15	1.327	0.00063	± 0.00001	0.29569	± 0.00516			0.31982	1.325
448.15	3.657	0.00369	± 0.00004	0.71000	± 0.00414			0.71835	3.578
448.15	7.565	0.00861	± 0.00011	0.84269	± 0.00240			0.83881	7.660
448.15	10.497	0.01135	± 0.00018	0.88079	± 0.00216			0.86263	10.272
448.15	13.442	0.01413	± 0.00008	0.89333	± 0.00176			0.87578	13.275
448.15	17.459	0.01764	± 0.00006	0.89825	± 0.00257			0.88272	17.765

[a] x_1 denotes the mole fraction of component 1 (CO_2) in the water-rich liquid phase, x'_1 denotes the mole fraction of component 1 in the CO_2-rich liquid phase, and y_1 denotes the mole fraction of component 1 in the vapor phase. Superscripts ‘exp’ and ‘cal’ denote experimental and calculated values.

Table 2.
Thermodynamic properties for the pure compounds. [a]

Compound	T_c (K)	p_c (MPa)	ω
CO_2	304.13	7.3773	0.22394
H_2O	647.1	22.064	0.3443

[a] from REFPROP version 9.0 [26]

Table 3.
Parameters in Eqs 12 to 14 for CO_2 (1) + H_2O (2).

Parameter	Value	Parameter	Value
A	0.33810	D_{12}	18.664
B	-0.46426	D_{21}	3.720
C_0	-6.1384	E_{12}	-5549.77
C_1	42.842	E_{21}	-803.18
C_2	-44.358	F_{12}	-112.67
C_3	12.786	F_{21}	21.13

Table 4.
Average absolute relative deviations $\Delta p/p$ for pressure and average absolute deviations Δy_1 for mole fraction for CO_2 (1) + H_2O (2) using the $\gamma - \phi$ approach.[a]

T (K)	$\Delta p/p$	Δy_1
298.15	2.19 %	0.0005
323.15	2.73 %	0.0138
348.15	2.94 %	0.0097
373.15	2.80 %	0.0108
398.15	2.09 %	0.0091
423.15	1.96 %	0.0119
448.15	1.45 %	0.0146

[a] calculated average absolute deviations for pressure and vapor phase composition using the $\gamma - \phi$ approach

Table 5.
Calculated results with the Krichevsky-Kasarnovsky (KK) approach.

T (K)	H_{12} (MPa)	$\overline{V}_1^{\infty}$ (cm^3/mol)	$\Delta p/p$ % [a]
298.15	169.65	12.00	0.70
323.15	285.36	20.93	3.01
348.15	438.97	6.73	2.62
373.15	556.44	4.28	2.21
398.15	605.82	8.88	2.22
423.15	688.37	-12.46	2.40
448.15	635.12	36.91	2.23

[a] calculated average absolute deviations for pressure

Figure Captions

Fig. 1 Left: schematic diagram of the apparatus. Right: photograph of highpressure vessel showing the sapphire windows and swivel joint.

Fig. 2 Gas chromatography calibration results for CO_2 and H_2O

Fig. 3 Phase diagram for CO_2 (1) + H_2O (2) system at 298.15 K

Fig. 4 Phase diagram for CO_2 (1) + H_2O (2) system at 323.15 K

Fig. 5 Phase diagram for CO_2 (1) + H_2O (2) system at 348.15 K

Fig. 6 Phase diagram for CO_2 (1) + H_2O (2) system at 373.15 K

Fig. 7 Phase diagram for CO_2 (1) + H_2O (2) system at 398.15 K

Fig. 8 Phase diagram for CO_2 (1) + H_2O (2) system at 423.15 K

Fig. 9 Phase diagram for CO_2 (1) + H_2O (2) system at 448.15 K

Fig. 10 Henry's law constant *H* against system temperature

Fig. 11 *px* diagram for CO_2 (1) + H_2O (2) system: experimental data and calculated results with the $\gamma - \phi$ approach

Fig. 12 *py* diagram for CO_2 (1) + H_2O (2) system: experimental data and calculated results with the $\gamma - \phi$ approach

Fig. 13 Activity coefficient for CO_2 (1) and H_2O (2) in the saturated liquid phase at along representative isotherms.

Fig. 14 Calculation results using the Krichevsky-Kasarnovsky (KK) approach

Fig. 15 *px* diagram for CO_2 (1) + H_2O (2) system: experimental results and Duan's solubility correlation model

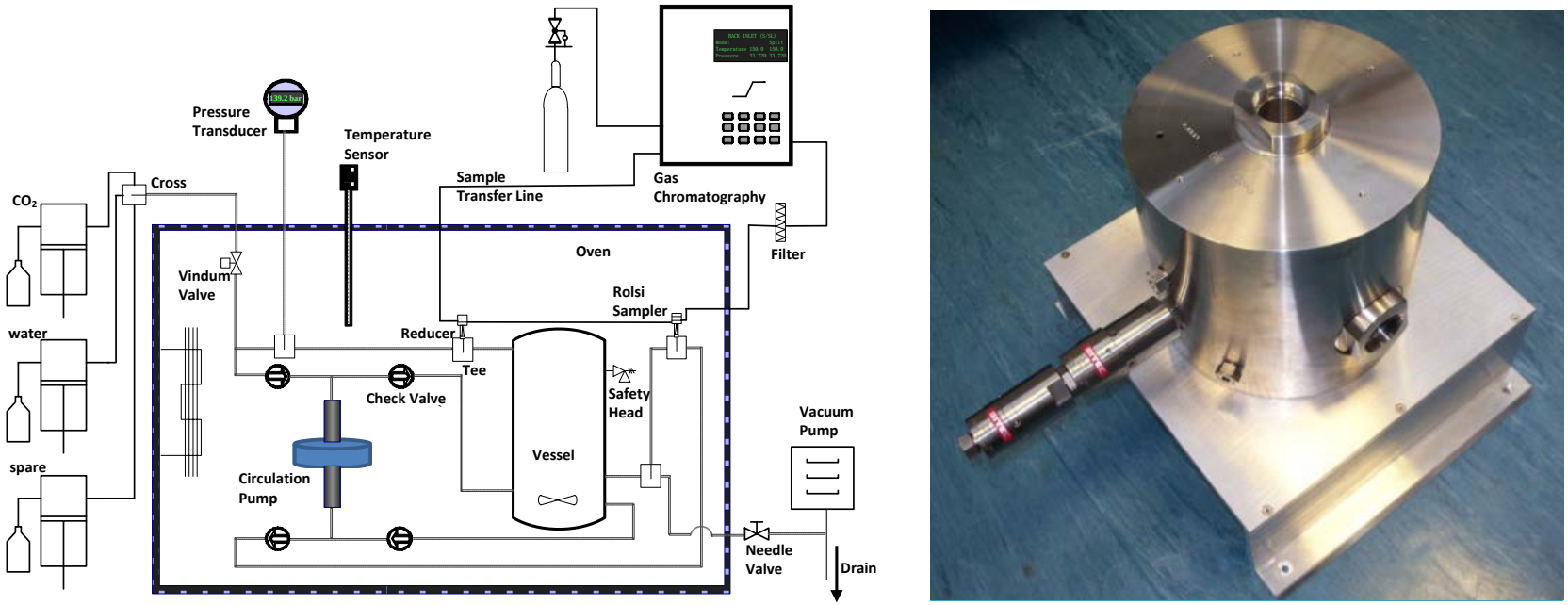

Fig. 1. Left: schematic diagram of the apparatus. Right: photograph of the high-pressure vessel showing the sapphire windows and swivel joint.

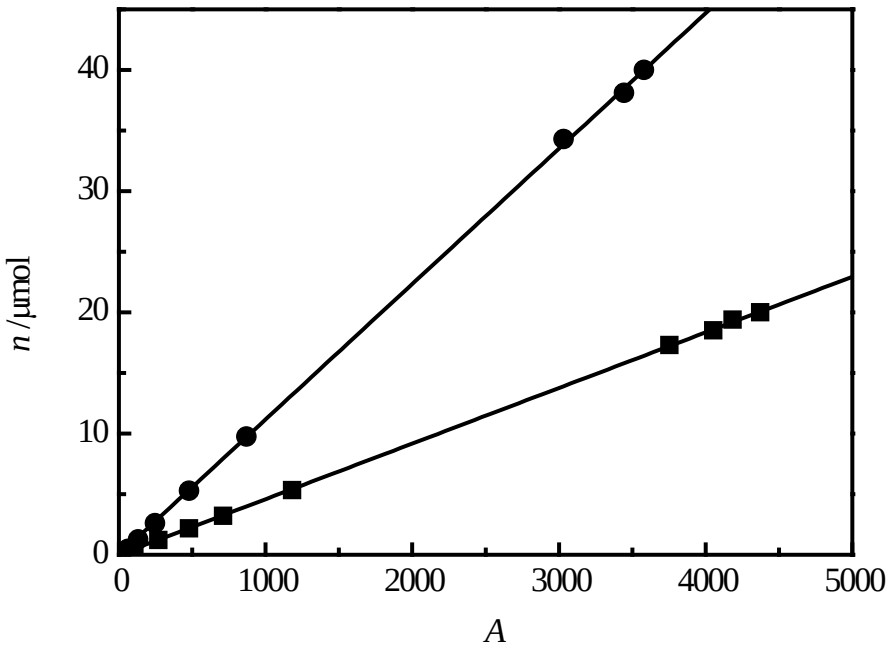

Fig. 2 Gas chromatography calibration results for CO_2 where n is the amount of substance injected and A is the dimensionless peak area determined from the chromatogram. ■, GC calibration data for CO_2; ●, GC calibration data for H_2O; —, linear correlation functions.

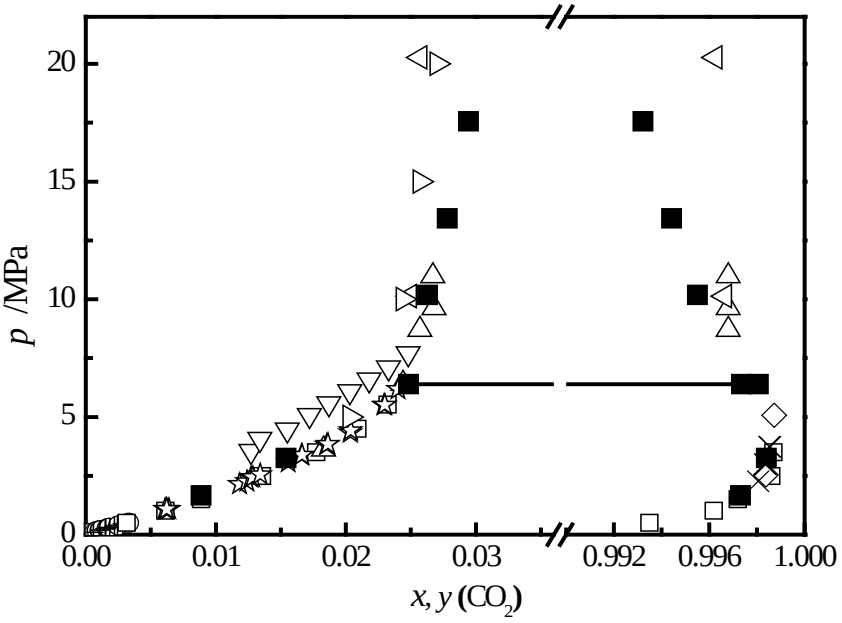

Fig. 3 Phase diagram for CO_2 (1) + H_2O (2) system at T = 298.15 K. ○, Campos et al. [37]; ＋, Dalmolin et al. [38]; □, Valtz et al. [23]; △, Nakayama et al. [39]; ▽, Vilcu and Gainar [40]; ☆, Zelvenskii [41]; ◇, Wiebe and Gaddy [42]; ×, Coan and King [43]; ◁, Gillespie and Wilson [44]; ▷, Teng et al.[45] ; ■, this work; —, three-phase tie line.

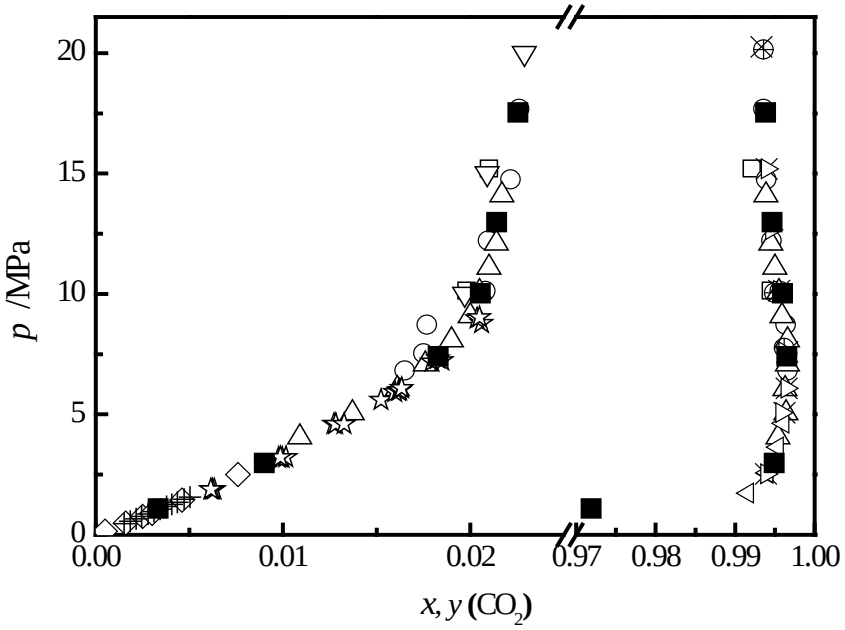

Fig. 4 Phase diagram for CO_2 (1) + H_2O (2) system at T = 323.15 K. □, D'Souza et al. [46]; ○, Briones et al. [47]; △ Bamberger et al. [30]; ▽, Bando et al. [48]; ◇, Zawisza and Malesinska [29]; ☆, Zelvenskii [41]; ＋, Fischer [49]; ×, Wiebe and Gaddy [42]; ⊕, Smith et al. [50]; ■, Coan and King [43]; ◁, Sidorov [51]; ▷, this work.

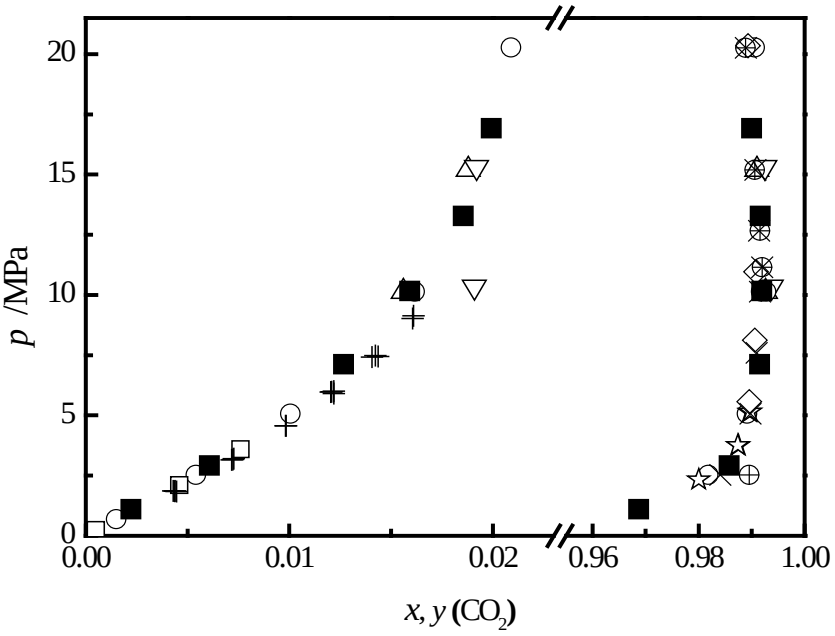

Fig. 5 Phase diagram for CO_2 (1) + H_2O (2) system at T = 348.15 K. △, D'Souza et al. [46]; ▽, Sako et al. [52]; ○, Gillespie and Wilson [44]; □, Zawisza and Malesinska [29]; +, Zelvenskii [41]; ☆, Coan and King [43]; ◇, Smith et al. [50]; ⊕, Wiebe and Gaddy [42]; × Sidorov et al. [51]; ■, this work.

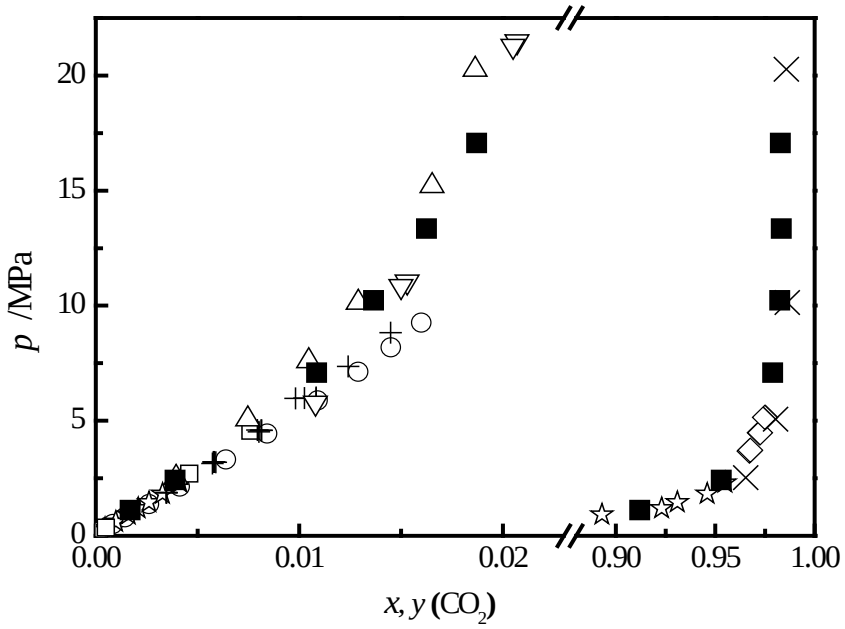

Fig. 6 Phase diagram for CO_2 (1) + H_2O (2) system at T = 373.15 K. □, Zawisza and Malesinska [29]; ○, Kiepe et al. [53]; ☆, Müller et al.[32]; ＋, Zelvenskii [41]; △, Wiebe and Gaddy [31]; ▽, Prutton and Savage [54]; ◇, King and Coan [43]; ×, Gillespie [44]; ■, this work.

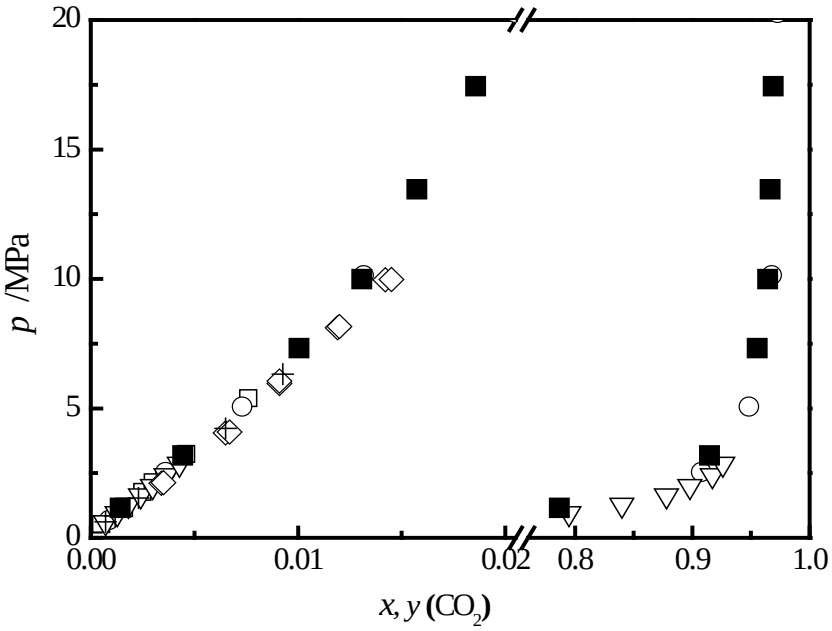

Fig. 7 Phase diagram for CO_2 (1) + H_2O (2) system at T = 398.15 K. □, Zawisza and Malesinska [29]; ○, Gillespie (at 394 K) [44]; ▽, Müller et al. (at 393 K) [32]; ◇, Nighswander (at 393 K) et al. [55]; ＋, Kiepe (at T = 393 K) [53]; ■, this work.

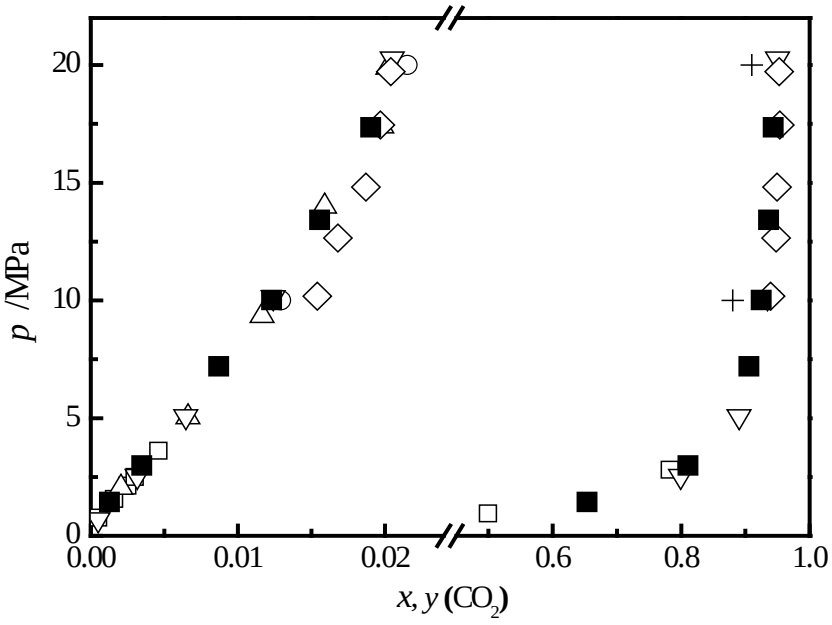

Fig. 8 Phase diagram for CO_2 (1) + H_2O (2) system at T = 423.15 K. □, Zawisza and Malesinska [29]; ○, Takenouchi and Kennedy [56]; △, Brunner [57]; ▽, Gillespie [44]; ＋, Takenouchi and Kennedy [58]; ◇, Sako et al. [52]; ■, this work.

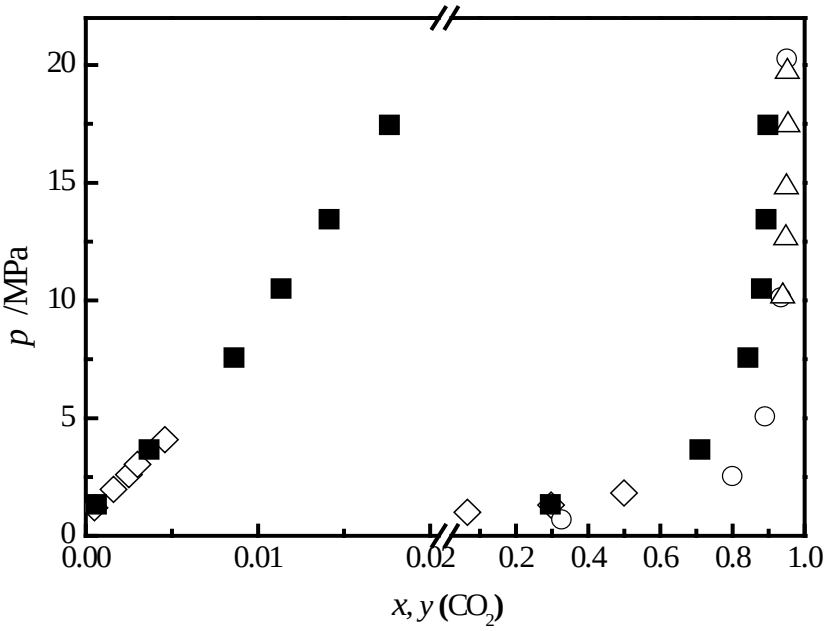

Fig. 9 Phase diagram for CO_2 (1) + H_2O (2) system at T = 448.15 K. ◇, Zawisza and Malesinska [29]; ○, Gilelspie (at T = 422 K) [44]; △; Sako et al. (at T = 421 K) [52]; ■, this work.

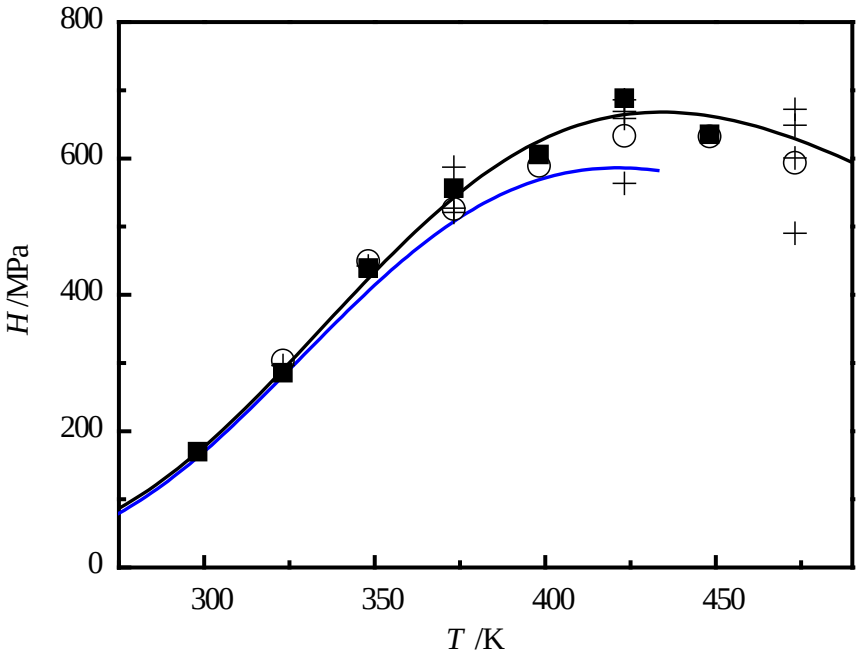

Fig. 10 Henry's law constant H_{12} as a function of temperature: —, this work using the $\gamma-\phi$ approach, Eq. (13); —, Correlation by Carroll et al. [8]; ■, this work using the KK approach; ○, Zawisza and Malesinska [29] (experimental); ＋, Zawisza and Malesinska [29] (correlation of literature data).

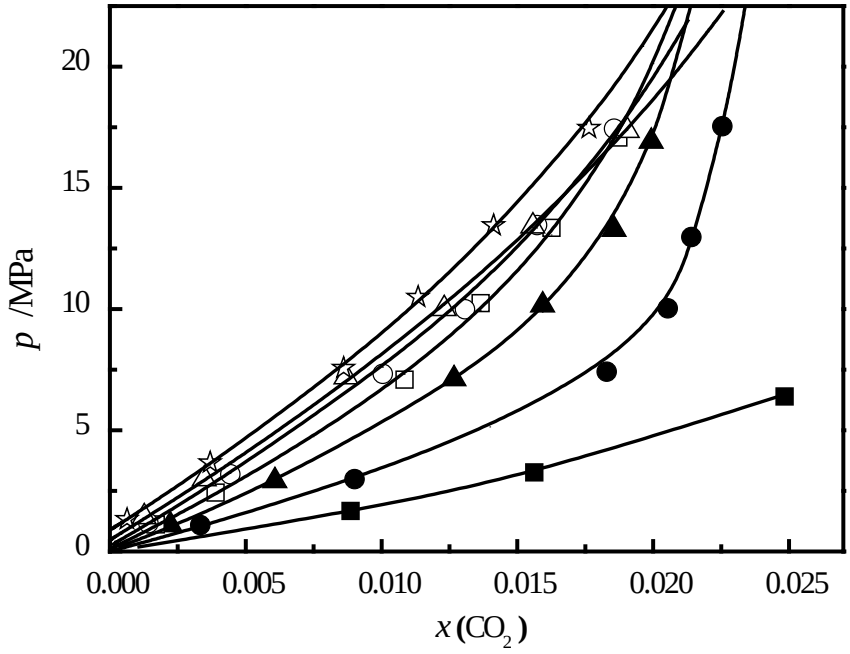

Fig.11 *p*-*x* diagram for CO_2 (1) + H_2O (2) system: experimental data and calculated results with the $\gamma-\phi$ approach. ■,*T* = 298.15 K; ●,*T* = 323.15 K; ▲,*T* = 348.15 K; □,*T* = 373.15 K; ○,*T* = 398.15 K; △,*T* = 423.15 K; ☆,*T* = 448.15 K.

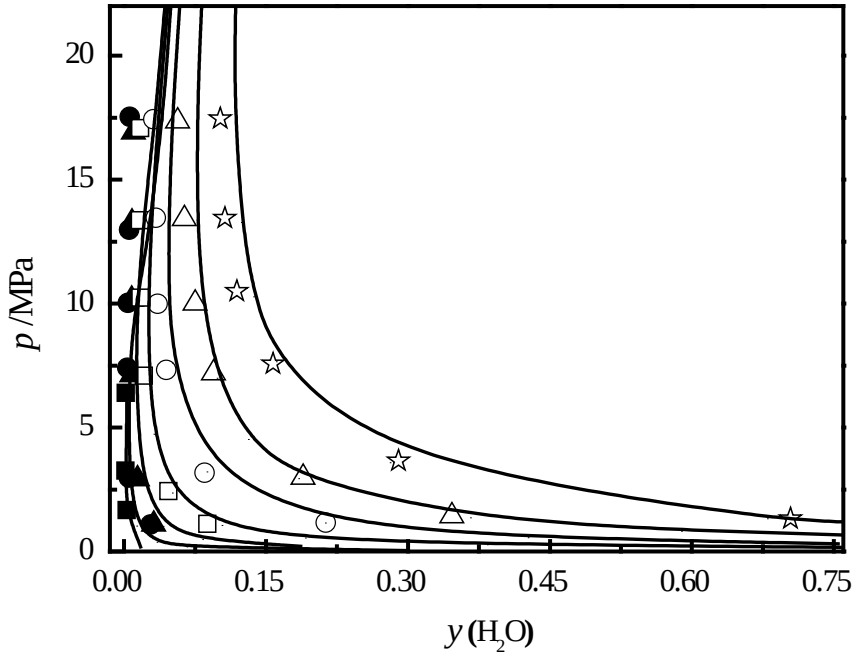

Fig. 12 *p-y* diagram for CO_2 (1) + H_2O (2) system: experimental data and calculated results with the $\gamma - \phi$ approach. ■, T = 298.15 K; ●,T = 323.15 K; ▲,T = 348.15 K; □,T = 373.15 K; ○,T = 398.15 K; △,T = 423.15 K; ☆,T = 448.15 K.

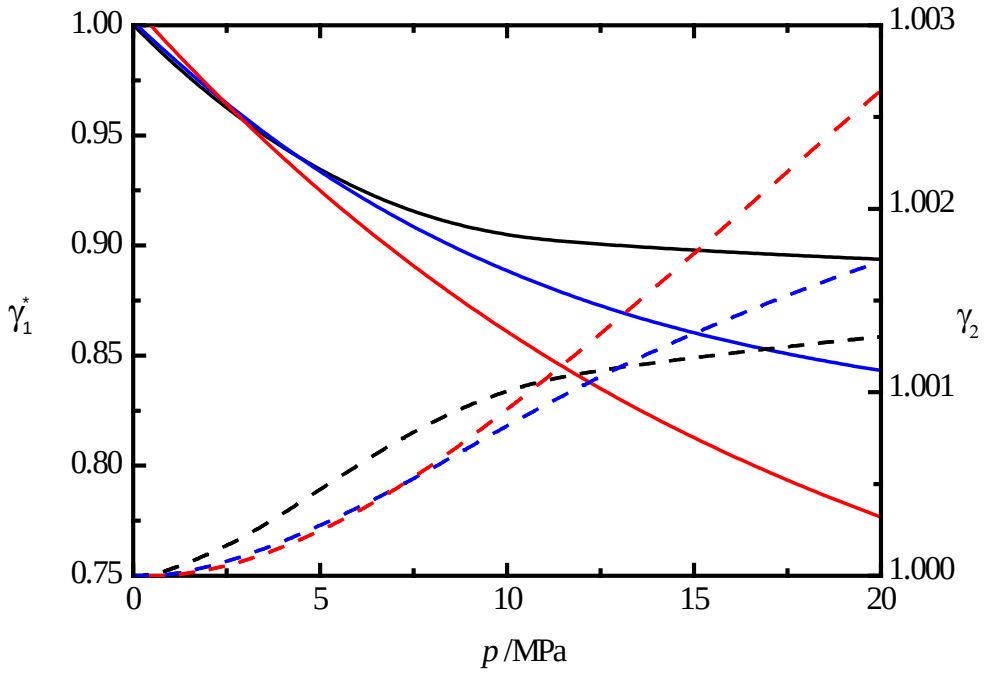

Fig. 13 Activity coefficient for CO_2 (1) and H_2O (2) in the saturated liquid phase on representative isotherms. γ_1^*: —, T = 323.15 K; —,T = 373.15 K; —,T = 423.15 K. γ_2: ---, T = 323.15 K; ---,T = 373.15 K; ---,T = 423.15 K.

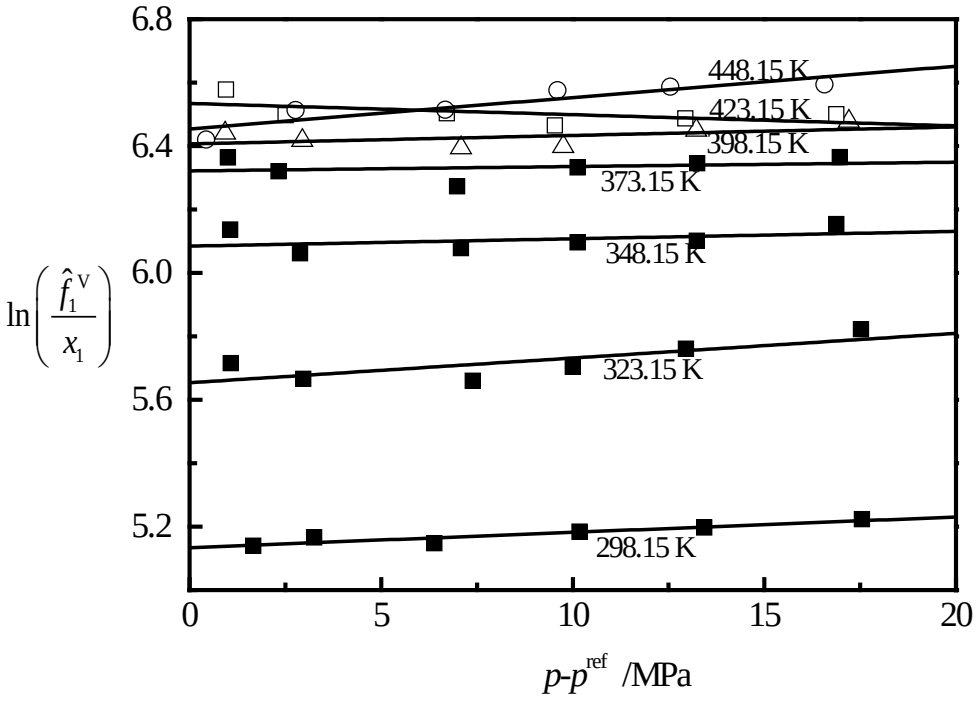

Fig. 14 Calculation results using the Krichevsky-Kasarnovsky (KK) approach

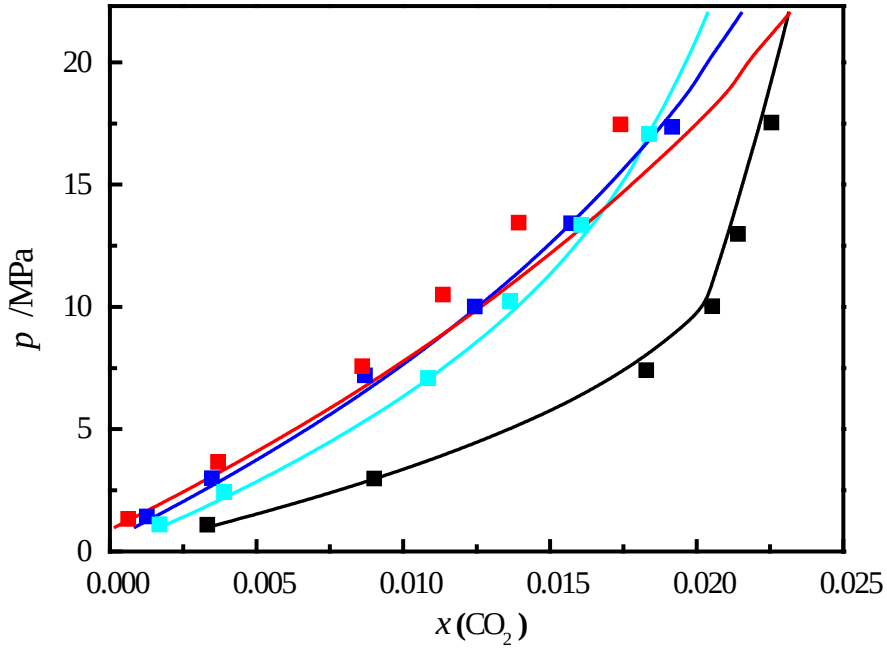

Fig. 15 *p-x* diagram for CO_2 (1) + H_2O (2) system. Experimental results (this work): ■,*T* = 323.15 K; ■,*T* = 373.15 K; ■,*T* = 423.15 K; ■,*T* = 448.15 K. Solubility model of Duan et al. [21]: —, *T* = 323.15 K; —, *T* = 373.15 K; —, *T* = 423.15 K; —, *T* = 448.15 K.